




Optical properties of niobium nitride plasmonic nanoantennas for the near- and mid-infrared spectral range

PHILIPP KARL,^{1,*}  MONIKA UBL,¹ MARIO HENTSCHEL,¹ PHILIPP FLAD,¹ ZONG-YI CHIAO,^{2,3} JING-WEI YANG,^{2,3} YU-JUNG LU,^{2,3} AND HARALD GIESSEN¹

¹4th Physics Institute and Research Center SCoPE, University of Stuttgart, Pfaffenwaldring 57, 70569 Stuttgart, Germany

²Research Center for Applied Sciences, Academia Sinica, Taipei 11529, Taiwan

³Department of Physics, National Taiwan University, Taipei 10617, Taiwan

*philipp.karl@pi4.uni-stuttgart.de

Abstract: Investigating new materials plays a very important role for advancing the field of nanofabrication and nanoplasmonics. Even though niobium nitride (NbN) is mainly known for its superconducting properties when fabricating superconducting nanowire single-photon detectors, we demonstrate that it is also a material for plasmonic nanoantenna applications. In this work we measure physical properties of thin NbN films, such as permittivity and superconductivity, and demonstrate the feasibility and tuning of the plasmonic nanoantenna resonance throughout the near- and mid-infrared spectral range. Therefore, we fabricate NbN structures, using electron beam lithography in combination with Ar ion-beam etching. Additionally, we determine the refractory properties of the NbN nanoantennas, namely their high temperature stability. We find that they are stable up to 500°C under ambient conditions. These aspects make them attractive for a multitude of plasmonic applications ranging from refractory emitters/absorbers to candidates for plasmonically improved superconducting single-photon detectors.

© 2020 Optical Society of America under the terms of the [OSA Open Access Publishing Agreement](#)

1. Introduction

Recently, a number of different optical applications for plasmonic nanostructures [1,2] such as thermophotovoltaics [3], heat transfer systems [4], plasmonic-based solar cells [5], nonlinear optics [6,7], different detectors for gas sensing [8–11] and single-photon detectors [12–14] have been introduced. In many devices light is efficiently absorbed and converted into heat [15], or nanostructures are used for selective emission for thermal radiation [16–19].

The materials used for the aforementioned applications are almost exclusively noble metals such as silver [20,21] and gold (Au) [22] due to their superb optical properties, which allow spectrally narrow and well-modulated plasmon resonances [23,24]. While at room temperature gold exhibits a good chemical stability, it starts to deform at higher temperatures unless a protection layer is used [25,26], which limits the use of gold for these applications. This is where other materials with good plasmonic properties are required [27], which can provide well-modulated plasmon resonances even under harsh conditions [28–30] or support the resonances with other interesting properties such as superconductivity at low temperatures.

For high temperature plasmonic applications one can use so-called refractory materials [31,32]. Due to their high melting point above 2000°C, these materials can be used for high temperature plasmonics. Materials associated with this group are for example tungsten [33], different nitrides [34], such as zirconium nitride [35,36], titanium nitride (TiN) [36–40], titanium oxynitride [41,42] and niobium (Nb) [43].

For new low temperature applications one can use materials with superconducting properties like Nb [13,43] to fabricate superconducting single-photon detectors, which can be enhanced by the plasmonic properties of the material.

Niobium nitride (NbN) can be associated with the group of refractory plasmonic materials, with a melting point of 2573°C and similar optical properties as Au, Nb, and TiN in the near-infrared. It shares the high durability of Nb and TiN at higher temperatures. Furthermore, it exhibits superior superconducting properties with a critical temperature (T_c) of 16.5 K. These characteristics makes it an interesting material for plasmonic applications such as plasmon-based superconducting single-photon detectors, which can be used for applications in quantum technology, e.g. quantum cryptography [44].

In this work we measure the physical properties of thin NbN films, namely permittivity and superconductivity. This enables us to perform simulations on plasmonic properties for our NbN films. With this data we fabricate NbN nanoantenna arrays, using electron beam lithography in combination with Ar ion-beam etching, which gives excellent control over the fabricated geometry, to demonstrate the tuning of the plasmonic nanoantenna resonance throughout the near- and mid-infrared spectral range. Furthermore, we demonstrate the temperature stability of our NbN nanoantennas under ambient conditions up to 500°C.

2. Physical properties of thin NbN films

By measuring the optical properties of thin films, predictions about the plasmonic properties of nanostructures of this material can be inferred. The refractive index and in addition the dielectric function can be measured using ellipsometry techniques.

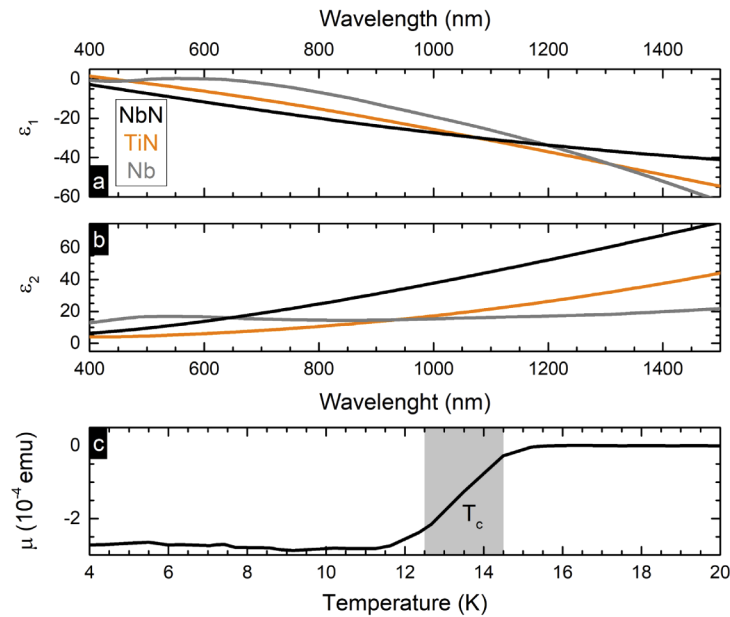


Fig. 1. Permittivity of NbN: Data are extracted from ellipsometry measurements of 50 nm thick NbN films on MgO substrate. In (a) and (b) the real and imaginary part of the dielectric function are compared to other refractory materials like Nb and TiN [43]. (c) Magnetic moment of NbN for low temperatures: NbN is a superconductor with a relatively high critical temperature. To demonstrate the superconducting behavior, a 50 nm thick NbN film on a MgO substrate was measured in a superconducting quantum interference device. The critical temperature is around 13.5 K.

In Fig. 1(a) and (b) we plot the dielectric function of our thin NbN films on magnesium oxide (MgO) substrates and compare them with Nb and TiN, which are other promising plasmonic materials. In order to obtain the dielectric function from the ellipsometry data, a fit with a Drude model and two Lorentz oscillators was used, as well as a polished MgO substrate as reflection reference to take the reflection into account. For relatively narrow and well-modulated plasmon resonances a negative real and small positive imaginary part of the dielectric function is desirable.

Figure 1(a) compares the real part of the dielectric function of NbN, Nb, and TiN. We identify a negative behavior for NbN, as shown in [45–47] and in addition, a similar behavior of all three materials, in the near infrared spectral range. In Fig. 1(b) the imaginary parts are depicted. Comparing them we realize that losses in NbN are higher than in Nb and TiN, which leads to broader resonances in NbN. These higher losses can benefit some other practical plasmonic application [48], such as loss-induced heat applications [49].

Moreover, NbN has another promising property, which is superconductivity. The critical temperature of NbN ($T_c = 16.5$ K) is higher than Nb ($T_c = 9.25$ K), which makes it a good candidate for plasmonic single-photon detectors, because a higher critical temperature leads to more effective detectors, for example due to shorter recovery times. Figure 1(c) shows the magnetic moment of our 50 nm thick NbN film on a MgO substrate. We clearly identify the superconducting behavior below $T = 13.5$ K. This critical temperature is in the expected range, which is slightly below the bulk value, due to the fact that the critical temperature of thin films is in generally lower than its literature bulk value [50,51]. The measurement was carried out with a superconducting quantum interference device (SQUID).

3. Fabrication of nanoantennas

To achieve the most advantageous optical properties for the NbN nanoantennas we need precisely defined structures. To obtain this quality for our nanoantennas we use electron beam lithography in combination with Ar ion-beam etching, which allows us to completely control the fabrication process. In Fig. 2 we present a schematic sketch of this process.

The plasmonic NbN film was sputter-deposited onto a MgO (100) substrate using radio-frequency magnetron sputtering, with a NbN target, a power of 120 W, a chamber pressure of $< 6 \times 10^{-8}$ torr, a deposition temperature of 800°C and with a nitrogen/argon flow rate of 1/24. We note that the properties of the metal nitride film can be varied with the argon/nitrogen flow rate, target, power, and growth temperature, compare Fig. 5 [52]. After the deposition, the chamber is vented with nitrogen at room temperature. These growth parameters ensure the highest possible critical temperature.

Afterwards a double layer positive photoresist system (200R and 950K Poly(methyl methacrylate, Allresist) and Spacer (Showa Denko) is spin-coated on top, see Fig. 2(a). In Fig. 2(b) the photoresist is exposed via electron beam patterning (eLine Plus, Raith) to create an inverse image of the desired nanostructure, after a development process. Figure 2(c) and (d) show the evaporation and lift-off, of the Chromium (Cr) etching mask. The Cr is evaporated via electron gun evaporation and the undesired Cr is afterwards removed with the lift-off process, using a *n*-ethyl-2-pyrrolidone based remover (Allresist), leaving the finished Cr etching mask on the NbN film. The surrounding NbN is removed via Ar ion-beam etching, see Fig. 2(e). In the last step the Cr is removed via a commercial Cr remover, see Fig. 2(f). An exemplary representation of the fabricated NbN nanoantennas is shown in Fig. 2(g), using a scanning electron microscope (SEM) (S-4800, Hitachi). The process yields high-quality nanoantenna arrays and allows for simple changing of their length and width, which enables us to tune the plasmonic nanoantenna resonance. This characteristic allows adjusting the near- and mid-infrared absorption, which is desired for photon absorption-based devices [9,53].

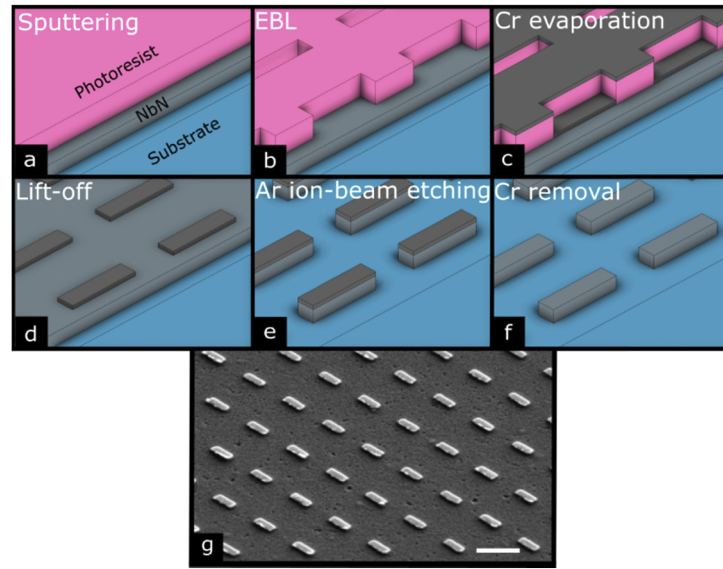


Fig. 2. Fabrication scheme of NbN nanoantennas: (a) 50 nm thick NbN films are sputtered onto a substrate and a layer of photoresist is spin-coated on top. (b) An inverse pattern of the nanostructure is created with electron beam lithography (EBL) exposure and development processes. (c) A Cr layer is evaporated on top of the structure. (d) The lift-off process removes the photoresist and provides the Cr etching mask. (e) With Ar ion-beam etching, the nanoantennas are transferred to the NbN film. (f) The Cr mask is removed with chemical Cr removal. (g) Exemplary representation of the finished NbN nanoantennas, the line represents a length of 500 nm.

4. Simulation and measurement of the transmission spectra

In Fig. 3 we plot the resulting transmission spectra of our rod-shaped nanoantennas for an electric field with a polarization along the long axis of the nanoantennas, with different lengths and periodicities and normal incidence for the simulations as well as the measurements. The upper row shows the simulation using extrapolated ellipsometry data and the lower row presents the measurement of the fabricated 50 nm thick NbN nanoantenna arrays. Figure 3(a) and (b) depict spectra of nanoantenna arrays with a length between 200 and 400 nm, a width of 100 nm, and a constant x- and y-periodicity of 500 nm. Figure 3(c) and (d) present spectra of nanoantenna with a length between 400 and 900 nm, a width of 200 nm, and a constant x- and y-periodicity of 1000 nm.

For the simulation we use an in-house implementation of the Fourier modal method with a scattering matrix approach and 225 plane waves [54,55], where we utilize air (refractive index of $n = 1$) as upper material and MgO (refractive index of $n \approx 1.7$) as substrate to match the conditions of the real samples. Figure 3(a) and (c) confirm tunable, relatively narrow and well-modulated plasmon resonances, which are fundamental nanoantenna dipole resonances [56], between wavelengths of 900 and 3000 nm, with an increasing modulation depth of up to 80%, which becomes larger with the antenna length. This can be explained via the larger dipole moments and resulting in an higher interaction strength. Moreover, the plasmonic nanoantenna resonance is tunable with the length of the antennas and shifts red for longer antennas. Other phenomena which can be observed in the simulated spectra are the sharp Rayleigh anomalies at 850 nm (Fig. 3(a)) and 1700 nm (Fig. 3(c)). This is caused by the perfect geometry, periodicity

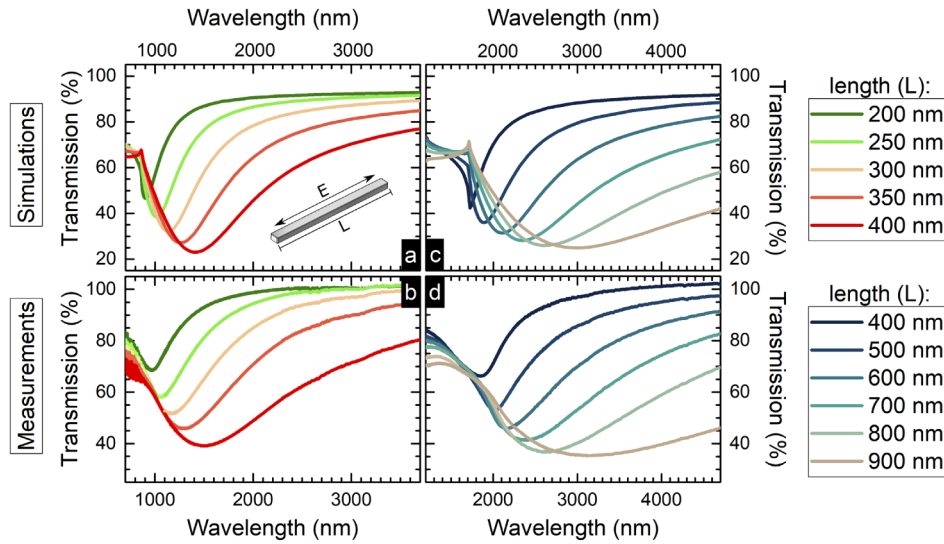


Fig. 3. Simulations (upper row) and measurements (lower row) of the plasmonic nanoantenna resonance of 50 nm thick NbN nanoantenna arrays. The simulations and measurements confirm relatively narrow and well-modulated plasmon resonances in the near- and mid-infrared. (a) and (b) show nanoantennas with a length between 200 and 400 nm, a width of 100 nm, and a constant x- and y-periodicity of 500 nm. (c) and (d) are nanoantennas with a length between 400 and 900 nm, a width of 200 nm, and a constant x- and y-periodicity of 1000 nm.

and boundary condition of the simulation, which leads to a strong diffraction at 90° angle, such strong anomalies typically only occur in simulations.

Figure 3(b) and (d) plot the measured transmission spectra of our NbN nanoantenna arrays. These results were obtained by a Fourier-transform infrared spectroscopy spectrometer (FTIR) (Bruker Vertex 80 microscope Hyperion 3000). The tunable, relatively narrow, and well-modulated plasmon resonances appear here as well and we obtain a good agreement between the simulation and the real samples. There are only small mismatches regarding modulation depth and width of the resonances, caused by a slightly imperfect geometry.

5. Refractory properties under ambient conditions

For refractory materials the stability at high temperatures is crucial. NbN bulk exhibits a high stability at these temperatures due to its melting point of 2573°C and internal oxidation temperature of 800°C . However, it should be noted that the nanoscale regime in combination with high temperatures is able to change the plasmonic properties of our antennas due to an alteration of their optical properties [57].

To further improve the high temperature stability of our nanoantennas we cover them with a protection layer. We use a 10 nm thin layer of alumina oxide (Al_2O_3), which we deposit via atomic layer deposition (R-200 Advanced, Picosun). This has different advantages. First it acts as protective layer and protects the shape of our nanoantennas [25]. Additionally, it prevents oxidation [57] while performing measurements under ambient conditions. Although NbN has an internal oxidation temperature of 800°C , surface oxidation already occurs at lower temperatures. The Al_2O_3 cover ensures the best possible temperature stability, both physically and chemically.

To investigate and demonstrate the high temperature stability and the plasmonic properties of our NbN nanoantennas, we have annealed the sample step by step up to 600°C and studied the

transmission of the nanoantenna arrays via FTIR spectrometer between each temperature step, at room temperature, to prevent temperature dependent changes of the permittivity during the measurement [58]. The dark green curve in Fig. 4(a) represents the transmission of a 700 nm long NbN nanoantenna array covered with 10 nm Al_2O_3 . We have annealed the nanoantennas for 45 min at 100°C under ambient conditions and measured the transmission again. After the annealing process the modulation depth decreases by 10%. This change can be explained by the modified optical properties of the NbN due to the fact that the shape of the nanoantenna remains the same, even at higher temperatures, see Fig. 4(b) and (c). Furthermore, there is no frequency shift observed after the annealing process. Repeating the same process with 200°C, 300°C and 400°C, leads to identical transmission spectra for these temperatures, see Fig. 4(a). This proves the fact that the NbN nanoantennas are stable over time and temperatures in this regime once they have been annealed for the first time. After annealing the sample for 45 min at 500°C the modulation depth decreases slightly, but with no shift in the resonance frequency. At 600°C in ambient condition the plasmon resonance nearly vanishes.

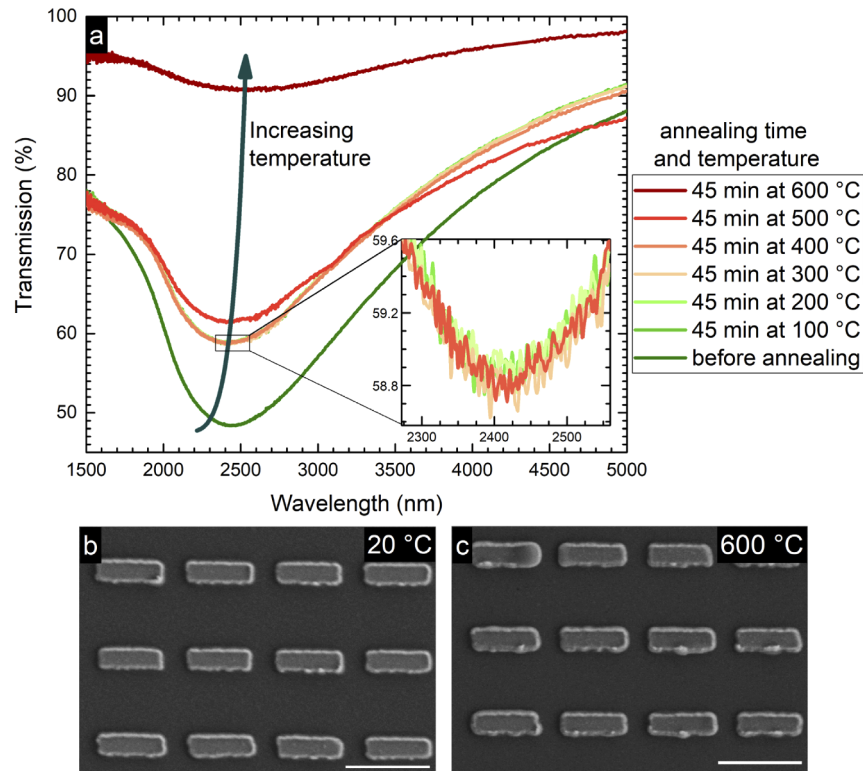


Fig. 4. High-temperature plasmonic properties and stability of the NbN nanoantennas on a MgO substrate, covered by a protective 10 nm Al_2O_3 layer. (a) The relative transmittance spectrum of the 700 nm long NbN nanoantenna array measured at room temperature. The sample was annealed for 45 min at different temperatures, in ambient conditions. The dark green curve depicts the plasmonic nanoantenna resonance before annealing and the other curves describe the resonances after annealing the sample. The spectra exhibit a decrease in the modulation depth after the first annealing. Followed by a constant resonance for temperatures up to 400°C. At 500°C the modulation depth decreases slightly and starts to disappear at 600°C. (b) and (c) show the NbN nanoantennas at 20°C and 600°C, the lines represent a length of 1000 nm. The shape of the nanoantennas at 600°C is the same as at 20°C.

By comparing the SEM images of the NbN nanoantenna arrays at 20°C and 600°C, see Fig. 4(b) and (c), we realize that the geometry of the antennas remains the same. This demonstrates the temperature stability of the geometry. Deterioration of the plasmonic properties is therefore likely due to the oxidation and formation of niobium oxynitride, due to the fact that an increase of oxygen content in our sample leads to a progressive change of the optical properties from those of NbN to those of the corresponding oxide [59].

6. Conclusion

In summary, we have fabricated NbN nanoantennas using electron beam lithography in combination with Ar ion-beam etching. The NbN nanoantennas exhibit tunable plasmon resonances in the near- and mid-infrared spectral range. In addition, the thin films possess a superconducting state at low temperatures, with a critical temperature of around 13.5 K, which makes them a promising candidate for plasmonically improved superconducting single-photon detectors, by using a perfect absorber [60] structure to further increase the plasmonic absorption. By utilization the high melting and oxidation temperature of NbN, we have demonstrated the refractory functionality of our nanoantennas, covered by 10 nm Al₂O₃, up to 500°C in ambient condition, which enables the use of NbN for refractory plasmonic applications.

Appendix

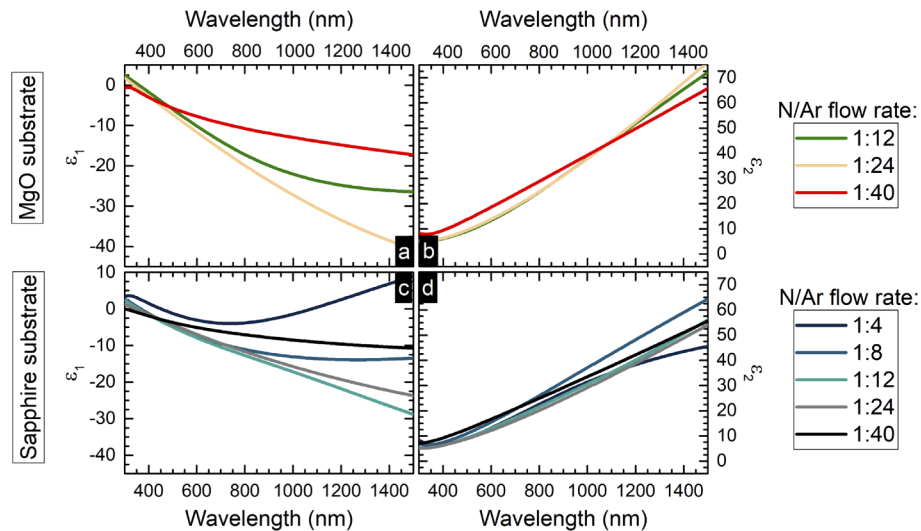


Fig. 5. Permittivity of NbN for different nitrogen/argon flow rates during the sputtering process. Data are extracted from ellipsometry measurements of approximately 50 nm thick NbN films on MgO substrates (upper row) and sapphire substrates (lower row). The left side draws the real part of the dielectric function and the right side the imaginary part. The nitrogen/argon flow rate as well as the substrate shows a strong influence on the real part of the dielectric function. The imaginary part, however, behaves similarly.

Funding

Academia Sinica (AS-CDA-108-M08); Ministry of Science and Technology, Taiwan (MOST-106-2112-M-001-036-MY3, MOST-109-2112-M-001-043-MY3); Ministerium für Wissenschaft, Forschung und Kunst Baden-Württemberg (IQST); Baden-Württemberg Stiftung; Carl-Zeiss-Stiftung; Deutsche Forschungsgemeinschaft; European Research Council (Complexplas).

Acknowledgments

We thank B. Miksch from the 1st Physics Institute (University of Stuttgart) for help with the SQUID measurements and T. Weiss from the 4th Physics Institute (University of Stuttgart) for help with the S-Matrix simulations.

Disclosures

The authors declare no conflicts of interest.

References

1. S. Aksu, A. A. Yanik, R. Adato, A. Artar, M. Huang, and H. Altug, "High-throughput nanofabrication of infrared plasmonic nanoantenna arrays for vibrational nanospectroscopy," *Nano Lett.* **10**(7), 2511–2518 (2010).
2. M. Rahmani, B. Luk'yanchuk, and M. Hong, "Fano resonance in novel plasmonic nanostructures," *Laser Photonics Rev.* **7**(3), 329–349 (2013).
3. Y. Guo, S. Molesky, H. Hu, C. L. Cortes, and Z. Jacob, "Thermal excitation of plasmons for near-field thermophotovoltaics," *Appl. Phys. Lett.* **105**(7), 073903 (2014).
4. D. G. Cahill, P. V. Braun, G. Chen, D. R. Clarke, S. Fan, K. E. Goodson, P. Keblinski, W. P. King, G. D. Mahan, A. Majumdar, H. J. Maris, S. R. Phillpot, E. Pop, and L. Shi, "Nanoscale thermal transport. II. 2003–2012," *Appl. Phys. Rev.* **1**(1), 011305 (2014).
5. H. A. Atwater and A. Polman, "Plasmonics for improved photovoltaic devices," *Nat. Mater.* **9**(3), 205–213 (2010).
6. M. Hentschel, T. Utikal, H. Giessen, and M. Lippitz, "Quantitative modeling of the third harmonic emission spectrum of plasmonic nanoantennas," *Nano Lett.* **12**(7), 3778–3782 (2012).
7. H. Aouani, M. Rahmani, M. Navarro-Cía, and S. A. Maier, "Third-harmonic-upconversion enhancement from a single semiconductor nanoparticle coupled to a plasmonic antenna," *Nat. Nanotechnol.* **9**(4), 290–294 (2014).
8. E. Herkert, F. Sterl, N. Strohfeldt, R. Walter, and H. Giessen, "Low-cost hydrogen sensor in the ppm range with purely optical readout," *ACS Sens.* **5**(4), 978–983 (2020).
9. S. Bagheri, N. Strohfeldt, F. Sterl, A. Berrier, A. Tittl, and H. Giessen, "Large-area low-cost plasmonic perfect absorber chemical sensor fabricated by laser interference lithography," *ACS Sens.* **1**(9), 1148–1154 (2016).
10. M. Sturaro, E. Della Gaspera, N. Michieli, C. Cantalini, S. M. Emamjomeh, M. Guglielmi, and A. Martucci, "Degenerately doped metal oxide nanocrystals as plasmonic and chemoresistive gas sensors," *ACS Appl. Mater. Interfaces* **8**(44), 30440–30448 (2016).
11. A. Tittl, P. Mai, R. Taubert, D. Dregely, N. Liu, and H. Giessen, "Palladium-based plasmonic perfect absorber in the visible wavelength range and its application to hydrogen sensing," *Nano Lett.* **11**(10), 4366–4369 (2011).
12. A. Eftekharian, H. Atikian, and A. H. Majedi, "Plasmonic superconducting nanowire single photon detector," *Opt. Express* **21**(3), 3043 (2013).
13. A. Farag, M. Ubl, A. Konzelmann, M. Hentschel, and H. Giessen, "Utilizing niobium plasmonic perfect absorbers for tunable near- and mid-IR photodetection," *Opt. Express* **27**(18), 25012 (2019).
14. C. M. Natarajan, M. G. Tanner, and R. H. Hadfield, "Superconducting nanowire single-photon detectors: Physics and applications," *Supercond. Sci. Technol.* **25**(6), 063001 (2012).
15. G. Baffou, R. Quidant, and F. Javier García De Abajo, "Nanoscale control of optical heating in complex plasmonic systems," *ACS Nano* **4**(2), 709–716 (2010).
16. E. Rephaeli and S. Fan, "Absorber and emitter for solar thermo-photovoltaic systems to achieve efficiency exceeding the Shockley-Queisser limit," *Opt. Express* **17**(17), 15145 (2009).
17. J. H. Park, S. E. Han, P. Nagpal, and D. J. Norris, "Observation of Thermal Beaming from Tungsten and Molybdenum Bull 's Eyes," *ACS Photonics* **3**(3), 494–500 (2016).
18. S. E. Han and D. J. Norris, "Beaming thermal emission from hot metallic bull's eyes," *Opt. Express* **18**(5), 4829 (2010).
19. K. A. Arpin, M. D. Losego, A. N. Cloud, H. Ning, J. Mallek, N. P. Sergeant, L. Zhu, Z. Yu, B. Kalanyan, G. N. Parsons, G. S. Girolami, J. R. Abelson, S. Fan, and P. V. Braun, "Three-dimensional self-assembled photonic crystals with high temperature stability for thermal emission modification," *Nat. Commun.* **4**(1), 2630 (2013).
20. X. Wang, C. Santschi, and O. J. F. Martin, "Strong improvement of long-term chemical and thermal stability of plasmonic silver nanoantennas and films," *Small* **13**(28), 1700044 (2017).
21. J. H. Park, P. Ambwani, M. Manno, N. C. Lindquist, P. Nagpal, S. H. Oh, C. Leighton, and D. J. Norris, "Single-crystalline silver films for plasmonics," *Adv. Mater.* **24**(29), 3988–3992 (2012).
22. E. K. Payne, K. L. Shuford, S. Park, G. C. Schatz, and C. A. Mirkin, "Multipole plasmon resonances in gold nanorods," *J. Phys. Chem. B* **110**(5), 2150–2154 (2006).
23. A. G. Nikitin, T. Nguyen, and H. Dallaporta, "Narrow plasmon resonances in diffractive arrays of gold nanoparticles in asymmetric environment: Experimental studies," *Appl. Phys. Lett.* **102**(22), 221116 (2013).
24. A. S. Kumbhar, M. K. Kinnan, and G. Chumanov, "Multipole plasmon resonances of submicron silver particles," *J. Am. Chem. Soc.* **127**(36), 12444–12445 (2005).

25. G. Albrecht, S. Kaiser, H. Giessen, and M. Hentschel, "Refractory Plasmonics without Refractory Materials," *Nano Lett.* **17**(10), 6402–6408 (2017).
26. H. Petrova, J. P. Juste, I. Pastoriza-Santos, G. V. Hartland, L. M. Liz-Marzán, and P. Mulvaney, "On the temperature stability of gold nanorods: Comparison between thermal and ultrafast laser-induced heating," *Phys. Chem. Chem. Phys.* **8**(7), 814–821 (2006).
27. A. Boltasseva and V. M. Shalae, "All that glitters need not be gold," *Science* **347**(6228), 1308–1310 (2015).
28. G. V. Naik, J. Kim, and A. Boltasseva, "Oxides and nitrides as alternative plasmonic materials in the optical range [Invited]," *Opt. Mater. Express* **1**(6), 1090 (2011).
29. G. V. Naik, V. M. Shalae, and A. Boltasseva, "Alternative plasmonic materials: Beyond gold and silver," *Adv. Mater.* **25**(24), 3264–3294 (2013).
30. S. M. Choudhury, D. Wang, K. Chaudhuri, C. Devault, A. V. Kildishev, A. Boltasseva, and V. M. Shalae, "Material platforms for optical metasurfaces," *Nanophotonics* **7**(6), 959–987 (2018).
31. U. Guler, A. Boltasseva, and V. M. Shalae, "Refractory plasmonics," *Science* **344**(6181), 263–264 (2014).
32. P. Nagpal, D. P. Josephson, N. R. Denny, J. Dewilde, D. J. Norris, and A. Stein, "Fabrication of carbon/refractory metal nanocomposites as thermally stable metallic photonic crystals," *J. Mater. Chem.* **21**(29), 10836–10843 (2011).
33. K. A. Arpin, M. D. Losego, and P. V. Braun, "Electrodeposited 3D tungsten photonic crystals with enhanced thermal stability," *Chem. Mater.* **23**(21), 4783–4788 (2011).
34. P. Patsalas, N. Kalfagiannis, S. Kassavetis, G. Abadias, D. V. Bellas, C. Lekka, and E. Lidorikis, "Conductive nitrides: Growth principles, optical and electronic properties, and their perspectives in photonics and plasmonics," *Mater. Sci. Eng., R* **123**, 1–55 (2018).
35. U. Guler, G. V. Naik, A. Boltasseva, V. M. Shalae, and A. V. Kildishev, "Performance analysis of nitride alternative plasmonic materials for localized surface plasmon applications," *Appl. Phys. B* **107**(2), 285–291 (2012).
36. U. Guler, V. M. Shalae, and A. Boltasseva, "Nanoparticle plasmonics: Going practical with transition metal nitrides," *Mater. Today* **18**(4), 227–237 (2015).
37. S. Bagheri, C. M. Zgrabik, T. Gissibl, A. Tittl, F. Sterl, R. Walter, S. De Zuani, A. Berrier, T. Stauden, G. Richter, E. L. Hu, and H. Giessen, "Large-area fabrication of TiN nanoantenna arrays for refractory plasmonics in the mid-infrared by femtosecond direct laser writing and interference lithography [Invited]," *Opt. Mater. Express* **5**(11), 2625 (2015).
38. G. V. Naik, J. L. Schroeder, X. Ni, A. V. Kildishev, T. D. Sands, and A. Boltasseva, "Titanium nitride as a plasmonic material for visible and near-infrared wavelengths," *Opt. Mater. Express* **2**(4), 478 (2012).
39. W. Li, U. Guler, N. Kinsey, G. V. Naik, A. Boltasseva, J. Guan, V. M. Shalae, and A. V. Kildishev, "Refractory Plasmonics with Titanium Nitride: Broadband Metamaterial Absorber," *Adv. Mater.* **26**(47), 7959–7965 (2014).
40. L. Gui, S. Bagheri, N. Strohfeldt, M. Hentschel, C. M. Zgrabik, B. Metzger, H. Linnenbank, E. L. Hu, and H. Giessen, "Nonlinear Refractory Plasmonics with Titanium Nitride Nanoantennas," *Nano Lett.* **16**(9), 5708–5713 (2016).
41. L. Braic, N. Vasilantonakis, A. Mihai, I. J. Villar Garcia, S. Fearn, B. Zou, N. M. N. Alford, B. Doiron, R. F. Oulton, S. A. Maier, A. V. Zayats, and P. K. Petrov, "Titanium oxynitride thin films with tunable double epsilon-near-zero behavior for nanophotonic applications," *ACS Appl. Mater. Interfaces* **9**(35), 29857–29862 (2017).
42. A. Kharitonov and S. Kharintsev, "Tunable optical materials for multi-resonant plasmonics: from TiN to TiON [Invited]," *Opt. Mater. Express* **10**(2), 513 (2020).
43. S. Bagheri, N. Strohfeldt, M. Ubl, A. Berrier, M. Merker, G. Richter, M. Siegel, and H. Giessen, "Niobium as alternative material for refractory and active plasmonics," *ACS Photonics* **5**(8), 3298–3304 (2018).
44. M. E. Reimer, G. Bulgarini, N. Akopian, M. Hoeser, M. B. Bavinck, M. A. Verheijen, E. P. A. M. Bakkers, L. P. Kouwenhoven, and V. Zwiller, "Bright single-photon sources in bottom-up tailored nanowires," *Nat. Commun.* **3**(1), 737 (2012).
45. A. Semenov, B. Günther, U. Böttger, H. W. Hübers, H. Bartolf, A. Engel, A. Schilling, K. Ilin, M. Siegel, R. Schneider, D. Gerthsen, and N. A. Gippius, "Optical and transport properties of ultrathin NbN films and nanostructures," *Phys. Rev. B* **80**(5), 054510 (2009).
46. T. Wieduwilt, A. Tuniz, S. Linzen, S. Goerke, J. Dellith, U. Hübner, and M. A. Schmidt, "Ultrathin niobium nanofilms on fiber optical tapers - A new route towards low-loss hybrid plasmonic modes," *Sci. Rep.* **5**(1), 17060 (2015).
47. M. W. Konevicki, K. L. Westra, B. T. Sullivan, K. E. Kornelson, and M. J. Brett, "Optical constants of reactively-sputtered NbN films," *Thin Solid Films* **232**(2), 228–231 (1993).
48. J. C. Ndukaife, V. M. Shalae, and A. Boltasseva, "Plasmonics—turning loss into gain," *Science* **351**(6271), 334–335 (2016).
49. J. C. Ndukaife, A. V. Kildishev, A. G. A. Nnanna, V. M. Shalae, S. T. Wereley, and A. Boltasseva, "Long-range and rapid transport of individual nano-objects by a hybrid electrothermoplasmonic nanotweezer," *Nat. Nanotechnol.* **11**(1), 53–59 (2016).
50. S. J. Lee and J. B. Ketterson, "Critical sheet resistance for the suppression of superconductivity in thin Mo-C films," *Phys. Rev. Lett.* **64**(25), 3078–3081 (1990).
51. T. Shiino, S. Shiba, N. Sakai, T. Yamakura, L. Jiang, Y. Uzawa, H. Maezawa, and S. Yamamoto, "Improvement of the critical temperature of superconducting NbTiN and NbN thin films using the AlN buffer layer," *Supercond. Sci. Technol.* **23**(4), 045004 (2010).
52. Y. J. Lu, R. Sokhoyan, W. H. Cheng, G. Kafaie Shirmanesh, A. R. Davoyan, R. A. Pala, K. Thyagarajan, and H. A. Atwater, "Dynamically controlled Purcell enhancement of visible spontaneous emission in a gated plasmonic heterostructure," *Nat. Commun.* **8**(1), 1–8 (2017).

53. S. Bagheri, H. Giessen, and F. Neubrech, "Large-area antenna-assisted SEIRA substrates by laser interference lithography," *Adv. Opt. Mater.* **2**(11), 1050–1056 (2014).
54. T. Weiss, N. A. Gippius, S. G. Tikhodeev, G. Granet, and H. Giessen, "Efficient calculation of the optical properties of stacked metamaterials with a Fourier modal method," *J. Opt. A: Pure Appl. Opt.* **11**(11), 114019 (2009).
55. T. Weiss, G. Granet, N. A. Gippius, S. G. Tikhodeev, and H. Giessen, "Matched coordinates and adaptive spatial resolution in the Fourier modal method," *Opt. Express* **17**(10), 8051 (2009).
56. L. Novotny, "Effective wavelength scaling for optical antennas," *Phys. Rev. Lett.* **98**(26), 266802 (2007).
57. G. Albrecht, M. Ubl, S. Kaiser, H. Giessen, and M. Hentschel, "Comprehensive study of plasmonic materials in the visible and near-infrared: linear, refractory, and nonlinear optical properties," *ACS Photonics* **5**(3), 1058–1067 (2018).
58. S. S. Kharintsev, A. V. Kharitonov, A. M. Alekseev, and S. G. Kazarian, "Superresolution stimulated Raman scattering microscopy using 2-ENZ nano-composites," *Nanoscale* **11**(16), 7710–7719 (2019).
59. M. Fenker, H. Kappl, O. Banakh, N. Martin, and J. F. Pierson, "Investigation of Niobium oxynitride thin films deposited by reactive magnetron sputtering," *Surf. Coat. Technol.* **201**(7), 4152–4157 (2006).
60. K. Chen, R. Adato, and H. Altug, "Dual-band perfect absorber for multispectral plasmon-enhanced infrared spectroscopy," *ACS Nano* **6**(9), 7998–8006 (2012).